J. Electrochem. Sci. Eng. **15(3)** (2025) 2666; http://dx.doi.org/10.5599/jese.2666

Open Access : : ISSN 1847-9286
https://pub.iapchem.org/ojs/index.php/JESE

Original scientific paper

Electrodeposition of Ni-Co thin films from ammonia-chloride electrolyte

Aygun Oruj Zeynalova, Natavan Sharafaddin Soltanova, Ulviyya Magsud Gurbanova✉, Ruhangiz Gurmuz Huseynova, Akif Shikhan Aliyev and Dilgam Babir Tagiyev

Institute of Catalysis and Inorganic Chemistry, Ministry of Science and Education of the Republic of Azerbaijan, H. Javid 113, AZ 1143, Baku, Azerbaijan

Corresponding author: ✉uqurbanova92@gmail.com

Received: February 6, 2025; Accepted: March 11, 2025; Published: April 1, 2025

Abstract

This study presents the research results on the co-deposition of nickel and cobalt from an alkaline electrolyte containing glycine. For this purpose, cyclic and linear polarization curves of co-deposition were obtained at various cobalt concentrations, different potential sweep rates, and electrolyte temperatures. It was established that the co-deposition process occurs anomalously, with the cobalt content in the deposited films exceeding that of nickel. The deposits obtained under optimal conditions contained 37.25 % Ni and 51.43 % Co. The study of the effect of the potential sweep rate on the co-deposition process of nickel and cobalt revealed a linear relationship between the current peak value and the square root of the potential sweep rate. This indicates that the initial stage of Ni-Co co-deposition is controlled by the diffusion of the metal ions to the cathode surface. When recording polarization curves on a rotating disk electrode at different rotation speeds, the relationship between the current peak value and the square root of the electrode rotation speed was also linear at relatively low rotation speeds. However, at higher rotation speeds, the process was controlled by electrochemical polarization. The co-deposition of Ni with Co was confirmed through X-ray diffraction, scanning electron microscopy and energy-dispersive X-ray spectroscopy analyses. The investigation of the catalytic activity of Ni-Co deposits in a neutral medium (0.5 M Na_2SO_4) demonstrated that the amorphous thin films, not subjected to annealing, exhibited the best electrocatalytic properties for the hydrogen evolution reaction. The Tafel slope was determined to be 118 mV dec^{-1}.

Keywords

Cobalt-nickel alloy; co-deposition; alkaline-glycine electrolyte; hydrogen evolution; electrocatalysis

Introduction

Green hydrogen, produced through water electrolysis using renewable energy sources, is considered one of the ideal energy carriers and sustainable industrial raw materials [1]. Researchers

are actively searching for low-cost, highly active, and stable electrocatalysts for the hydrogen evolution reaction (HER) and oxygen evolution reaction (OER) [2]. To this end, many materials have been studied, such as oxides [3], nitrides [4,5], sulphides [6], and phosphides [7]. Catalysts based on Ni, Co, Mo, and Fe, particularly their oxides and hydroxides, are promising for use as electrocatalysts in water electrolysis due to their abundance. The work [8] pays special attention to water electrolysis using solar energy, including the development of photovoltaic (PV) electrolyser systems for water. Cobalt is known to form solid solutions with nickel across the entire composition range, enabling the synthesis and utilization of their properties over a broad spectrum [9]. Electrodeposition methods are frequently used to obtain surface coatings due to their simplicity and low cost. Nickel, nickel alloy, and various composite derivative coatings play a crucial role in the aerospace and automotive industries due to their excellent corrosion resistance and mechanical properties [10,11]. Compared to conventional Ni-based coatings, nickel-cobalt alloys offer an exceptionally wide range of applications, including magnetic and electrocatalytic materials, as well as anticorrosive and wear-resistant coatings [12,13]. The histomorphology and various properties of nickel-cobalt alloys with different compositions vary significantly, and any change in preparation parameters, such as the composition of the galvanic solution, pH, or current density, can alter the final composition ratio in the coating [14]. In works [15,16], the electrodeposition of nickel with molybdenum from a Watts alkaline electrolyte was investigated. The resulting Ni-Mo alloys exhibited high catalytic activity in neutral solutions.

In work [17], the influence of Co content on the electrochemical deposition mechanism of Ni-Co thin films was studied using cyclic voltammetry, chronoamperometry, and electrochemical impedance spectroscopy. The Ni-Co alloy exhibited a more pronounced (111) orientation compared to pure nickel and demonstrated superior corrosion resistance. In work [18], the authors used a new ionic liquid-1-(4-fluorobenzyl)-3-(4-phenoxybutil) imidazolium bromide [FPIM]Br-as an additive in the electrodeposition of cobalt and nickel from acidic sulphate baths and Watts baths. It was found that the electrodeposition of Co^{2+} and Ni^{2+} ions in the presence of [FPIM]Br leads to the formation of finer-grained deposits with increased current efficiency, hardness, and corrosion resistance.

The Ni-Co alloy was deposited from a choline chloride-ethylene glycol solution [19]. The voltammetry results showed that the reduction peak appeared in the range of -0.6 V to -1.13 V *vs*. SCE, corresponding to the co-deposition of Ni-Co. The electrodeposition of the Ni-Co alloy from choline chloride-ethylene glycol was an irreversible process controlled by the diffusion of the deposited ions. Chronoamperometry revealed that the electrodeposition of Ni-Co onto a glassy carbon electrode occurred *via* a mechanism of instantaneous nucleation and three-dimensional growth, and the microstructure and Co content in the Ni-Co alloy could be easily controlled by varying the deposition potential. The authors [20] investigated the process of pulse electrodeposition of Ni-Co alloys, with the primary goal being the control of thickness and the formation of compact layers with good adhesion to the substrate surface. The electrodeposition of Ni-Co alloys was carried out at a temperature of 35 °C from an electrolyte containing chlorides of the deposited metals. The electrolyte also included H_3BO_3, NH_4Cl, and $Na_3C_6H_5O_7$ as a complexing agent, with $C_{12}H_{25}OSO_3Na$ as a wetting agent. Copper disks with an area of 0.5 cm^2 were used as substrates, and a platinum sheet was used as the counter electrode. It was found that both the pulse duration and the peak current density influenced the structure and composition of the alloy. In work [21], a method was proposed for producing catalysts for the HER and OER reactions from Ni hydroxide with the dual metal Co, Fe on Ni foam, using NaH_2PO_4 and NaH_2PO_2 as additives. The electrode demonstrated high activity and stability for both HER and OER reactions. The authors of work [22] synthesized nano-sized nickel-

cobalt (Ni-Co) alloys by electrodeposition from a choline chloride-urea ionic liquid. By controlling the deposition potential, the authors not only effectively varied the cobalt content, microstructure, and crystal size of the Ni-Co alloy but also influenced the preferred orientation of the alloy in the (220) crystalline plane. Additionally, the Ni-Co alloy exhibited excellent corrosion resistance. Co-deposition of nickel and cobalt can be conducted from various electrolytes: sulphate, chloride, chloride-sulphate, or sulfamate solutions, with or without additives. Additives such as saccharin, sodium lauryl sulphate, boric acid, and ammonium sulphate are used to maintain the electrolyte pH at the required level [23]. In work [24], during the co-deposition of Ni with Zn, the addition of glycine did not alter the mechanism of the electrodeposition process, but it increased the current efficiency by approximately 6 %, presumably due to the reduction of the hydrogen evolution reaction contribution to the overall cathodic process rate. The addition of glycine improved the surface morphology of the synthesized coatings by reducing roughness, promoting a denser packing of the growing phase nuclei, and increasing the alloy's nickel content by an average of 4 at.%.

It is well known that cobalt and nickel form a series of stable solid solutions, and as the cobalt content increases in thin films, the magnetic properties, heat resistance, and hardness of the alloys improve. The objective of this study is to investigate the co-deposition of Ni-Co thin films from an alkaline electrolyte containing glycine, which exhibits both magnetic and electrocatalytic properties in the water-splitting reaction. In addition to the main components of the alloy, glycine was introduced into the electrolyte as a chelating additive, and ammonia was used to adjust the pH of the electrolyte to the desired value.

Experimental

The electrolyte was prepared by dissolving 0.8 M glycine in bi-distilled water, followed by the addition of the calculated amounts of $NiSO_4 \cdot 6H_2O$, $NiCl_2 \cdot 6H_2O$ and $CoCl_2 \cdot 6H_2O$. The pH of the electrolyte was adjusted to 9.5 by adding NH_4OH. Cyclic and linear polarization curves were recorded using the IVIUMSTAT Electrochemical Interface potentiostat, which allowed the determination of the potential range at which the co-deposition of nickel with cobalt occurs. Polarization measurements were conducted in a three-electrode electrochemical cell, with platinum (2 cm^2) as the working electrode, platinum (4 cm^2) as the auxiliary electrode, and a silver/silver chloride electrode with a saturated KCl solution as the reference electrode. All potential values presented in the article are referenced relative to this electrode. Polarization curves were also recorded using a rotating disk platinum electrode with a diameter of 0.5 cm and an area of 0.2 cm^2. The electrode rotation speed varied within the range of 900 to 3600 rpm.

To determine the elemental composition of films and their electrocatalytic properties, Ni-Co thin films were obtained in the galvanostatic mode in a two-electrode cell on nickel substrates with an area of 2 cm^2 at current densities of 10-25 mA cm^{-2} for 12-15 hours, at room temperature. A platinum foil with a surface area of 4 cm^2 was used as the anode. Before deposition, the nickel substrates were subjected to electrochemical polishing, followed by degreasing with alcohol and acetone. The deposited films were amorphous and subjected to annealing in air at 573 K for 1 hour, and then at 723 K for 1 hour. Some samples were also annealed in an argon atmosphere for 1 hour at 673 K. The surface morphology and elemental composition of the films were examined using a scanning electron microscope (SEM) model “Oxford Instruments,” and the elemental composition was determined by EDX. Structural analysis was carried out using a Rigaku X-ray diffractometer model “Miniflex-500” with CuKα radiation (λ = 0.154 nm). The electrocatalytic properties of the films

were investigated by recording polarization curves in a neutral 0.5 M Na_2SO_4 solution, followed by determining the Tafel slope of the curves.

Results and discussion

Before the studies on the co-deposition of cobalt with nickel, investigations were conducted on the deposition of individual alloy components from an alkaline-glycine electrolyte. It was found that the reduction of cobalt ions from the ammonia-glycine electrolyte occurs in two steps, at potentials of -0.45 V and, subsequently, at -0.65 V, where cobalt begins to co-deposit simultaneously with hydrogen evolution [25]. The oxidation of cobalt also occurs in two steps, at potentials of -0.75 V and -0.25 V, and the process is reversible.

Nickel electrodeposition, however, occurs in one step, beginning at a potential of -0.65 V, and continuing with simultaneous hydrogen evolution [26]. The oxidation of nickel occurs within a potential range of -0.65 V to -0.75 V, making the process also reversible. Glycine (H_2N-CH_2-COOH) is typically considered a dipolar ion, with its structure being either protonated or deprotonated depending on the pH of the solution [27], and the equilibrium between these forms is described by Equation (1)

$$H_2N\text{-}CH_2\text{-}COO^- \underset{OH^-}{\overset{H^+}{\rightleftharpoons}} {}^+H_3N\text{-}CH_2\text{-}COO^- \underset{OH^-}{\overset{H^+}{\rightleftharpoons}} {}^+H_3N\text{-}CH_2\text{-}COOH \quad (1)$$

Depending on the concentration of glycine, nickel, and the pH of the electrolyte, nickel in solution exists in various complexes. At pH 9, Ni^{2+} is predominantly found in the form of the [$NiGly_3$] complex, which exhibits high stability [28]. Conversely, cobalt forms coordination complexes with glycine in solution, which are formed as the pH increases [29,30]. Therefore, from a purely thermodynamic standpoint, glycine is expected to stabilize Co^{2+} in solution by negatively shifting the Co^{2+}/Co potential.

Figure 1 shows the cyclic polarization curve of the co-deposition of nickel with cobalt from an ammonia-alkaline electrolyte containing glycine.

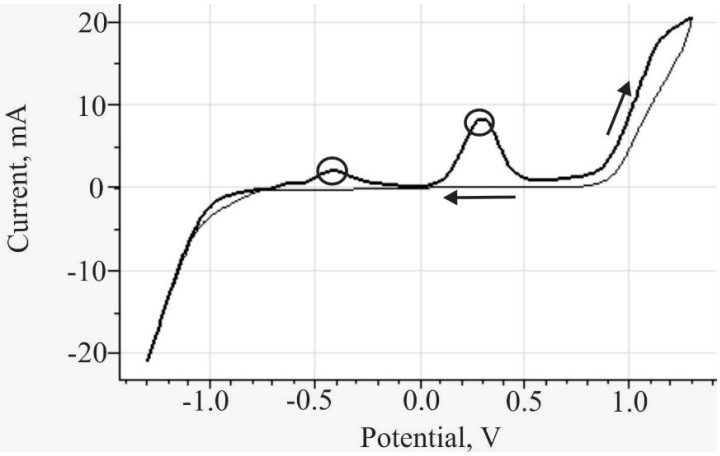

Figure 1. *Cyclic polarization curve of the co-deposition of nickel with cobalt in the potential range of 1.3 to -1.3 V. Electrolyte composition: 0.1 M $NiSO_4 \cdot 6H_2O$ + 0.1 M $NiCl_2 \cdot 6H_2O$ + 0.1 M $CoCl_2 \cdot 6H_2O$ + + 0.8 M $C_2H_5NO_2$, pH adjusted to 9.5 by adding NH_4OH, ν = 15 mV s^{-1},* T *= 298 K*

From the figure, it can be seen that when the curve is recorded down to a potential of -1.3 V, only one peak appears on the cathodic curve, corresponding to the co-deposition of nickel with cobalt occurring simultaneously with hydrogen evolution. On the anodic component of the cyclic polarization curve, two peaks are visible at potentials of -0.4 and +0.3 V. The first corresponds to the oxidation of the pure cobalt phase, while the second corresponds to the dissolution of the Ni-Co film. The co-deposition of these two metals and hydrogen evolution do not allow for a complete representation of the cathodic portion of this process. To investigate the initial stage of co-

deposition, linear polarization curves were recorded down to a potential of -0.7 V. From Figure 1, based on the positioning of the peaks of the cathodic and anodic processes, it can be concluded that the co-deposition of Ni with Co is an irreversible process.

Figure 2a presents the cyclic polarization curve of the co-deposition of nickel with cobalt from an alkaline glycine electrolyte on a platinum electrode, recorded down to a potential of -0.8 V.

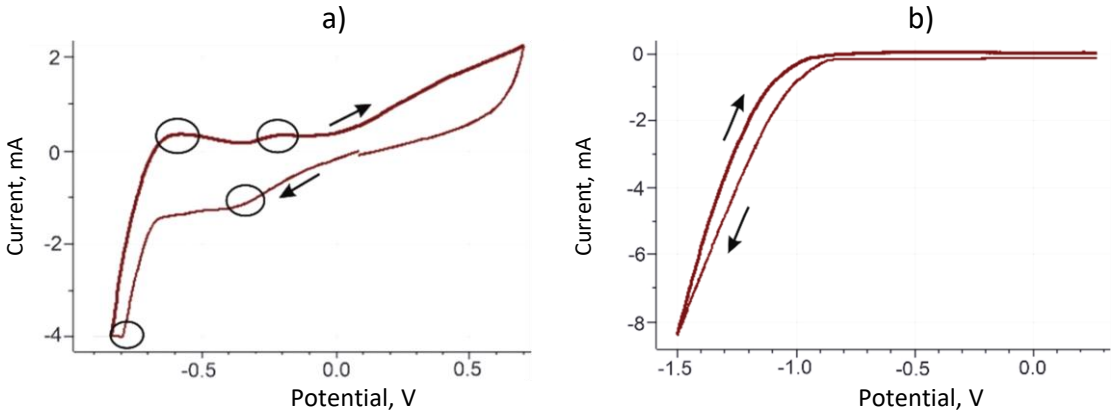

Figure 2. *a) Cyclic polarization curve of Ni-Co co-deposition from an alkaline glycine electrolyte on a platinum electrode: Electrolyte composition: 0.1 M $NiSO_4 \cdot 6H_2O$ + 0.1 M $NiCl_2 \cdot 6H_2O$ + 0.1 M $CoCl_2 \cdot 6H_2O$ + + 0.8 M $C_2H_5NO_2$, pH adjusted to 9.5 by adding NH_4OH,, ν = 15 mV s^{-1}, T = 298 K. b) Cyclic background curve of 0.8 M $C_2H_5NO_2$, pH adjusted to 9.5 by adding NH_4OH*

The polarization curve shows a single wave at potential values between -0.35 and -0.4 V. This wave corresponds to the initial stage of the co-deposition of nickel with cobalt. When polarization curves of co-deposition are recorded down to a potential of -1.3 V (Figure 1), this wave disappears, and it becomes difficult to capture the moment when deposition begins, as co-deposition occurs simultaneously with hydrogen evolution. Furthermore, the simultaneous reduction of both metals along with hydrogen leads to a change in the pH in the near-electrode space and the formation of hydroxides of the deposited metals, with co-deposition occurring then from their hydroxides. Figure 2b presents the cyclic polarization curve of the background electrolyte. The presence of glycine in the electrolyte prevents the formation of $Ni(OH)_x$ formation but does not affect Co(OH)x formation. The authors [31] attribute this to the complexation constants (β) during the formation of complexes of both metals with amino acids (βNi > βCo). When using glycine, regardless of the electrolyte pH and glycine concentration, the amount of Co in the deposited layer is usually significantly higher than that of the noble metal, in this case, nickel. This phenomenon during the co-deposition of two metals is referred to as "anomalous co-deposition" and was introduced by Brenner [32]. The anomalous co-deposition of thin Co-Ni alloy layers is explained by the formation of cobalt hydroxide on the cathode surface, which simultaneously accelerates the deposition of cobalt and reduces the deposition rate of nickel [33,34]. At pH values from 2 to 5, the reduction of Co is facilitated due to Co(OH)2 formation at the electrode/electrolyte interface. This is due to the competitive adsorption of hydroxides on the electrode surface, which helps to reduce the content of the less noble metal. In alkaline media, the concentration of $Co(OH)_2$ at the electrode/electrolyte interface decreases while $Ni(OH)_2$ increases, promoting the reduction of Ni in the coating [11]. In the anodic component of the polarization curve for co-deposition, at potentials from -0.85 to -0.5 V, the thin Ni-Co film dissolves, and at -0.2 V, cobalt oxidation as a separate phase takes place.

Figure 3 shows the linear polarization curve of the co-deposition of nickel with cobalt as a function of cobalt concentration in the electrolyte.

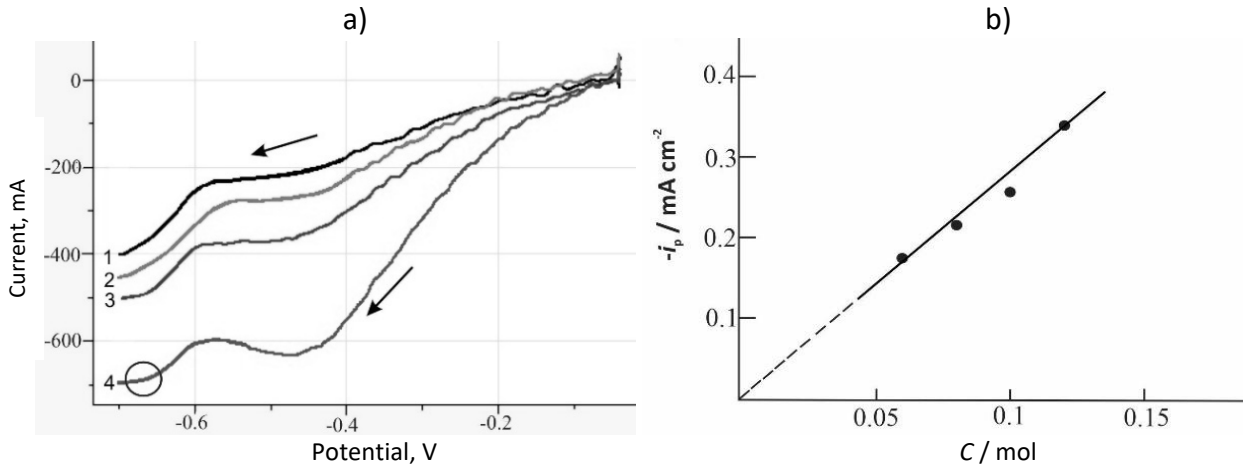

Figure 3. *a) Linear voltammogram of the co-deposition of nickel with cobalt as a function of cobalt concentration in the electrolyte. Electrolyte composition: 0.1 M $NiSO_4 \cdot 6H_2O$ + 0.1 M $NiCl_2 \cdot 6H_2O$ + 0.8 M $C_2H_5NO_2$, pH adjusted to 9.5 by adding NH_4OH, ν = 15 mV s^{-1}, T = 298 K. $CoCl_2 \cdot 6H_2O$ concentration: 1: 0.06 M; 2: 0.08 M; 3: 0.1 M and 4: 0.12 M; b) dependence of the current peak on the cobalt concentration in the electrolyte*

It is evident from the curves in Figure 3 that with increasing cobalt concentration in the electrolyte, the height of the wave at a potential of -0.4 V, corresponding to cobalt deposition, increases, which most likely leads to the formation of a larger amount of cobalt hydroxide in the near-electrode space. The height of the co-deposition peak at a potential of -0.7 V also increases but to a lesser extent than the cobalt reduction wave. The dependence of the co-deposition wave height on the cobalt concentration in the electrolyte is shown in Figure 3b; it is linear, which is typical for processes controlled by the diffusion of deposited ions.

When studying the effect of nickel concentration on the co-deposition process and the composition of the deposited films, the nickel concentration was varied from 0.8 to 1.2 M. It was found that the concentration of nickel in the electrolyte has little effect on both the co-deposition process and the composition of the deposited film. The cobalt content in the deposits always exceeded the nickel content, which is consistent with other studies on the co-deposition of nickel with cobalt [35,36].

Figure 4 shows the linear polarization curves of the co-deposition of nickel and cobalt at different potential sweep rates.

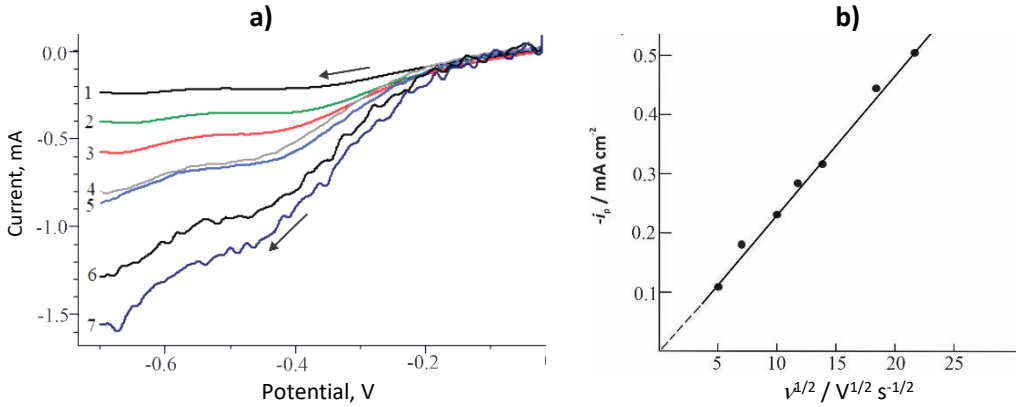

Figure 4. *a) Linear polarization curve of co-deposition of nickel with cobalt from an ammonia-chloride electrolyte at different potential sweep rates. Electrolyte composition: 0.1 M $NiSO_4 \cdot 6H_2O$ + 0.1 M $NiCl_2 \cdot 6H_2O$ + +0.1 M $CoCl_2 \cdot 6H_2O$ + 0.8 M $C_2H_5NO_2$, pH adjusted to 9.5 by adding NH_4OH, T = 298 K. Sweep rates: 1: 5; 2: 10; 3: 15; 4: 20; 5: 30; 6: 40 and 7: 50 mV s^{-1}. b) Dependence of peak current on the square root of sweep rate*

It can be observed from Figure 4 that as the potential sweep rate increases, the height of the co-deposition wave increases. Based on the data obtained from Figure 4a, the dependence of the peak current i_p on the square root of the sweep rate ($\nu^{1/2}$) was constructed, as shown in Figure 4b. The dependence of the limiting current on the potential square root of sweep during the initial stage of co-deposition follows a linear pattern, characteristic of processes controlled by diffusion kinetics.

Figure 5 shows linear polarization curves of co-deposition of nickel with cobalt at different deposition temperatures. Increasing the electrolyte temperature accelerates the co-deposition process, facilitating the reduction of the deposited metals, which leads to a slight shift of the co-deposition potential towards more positive values.

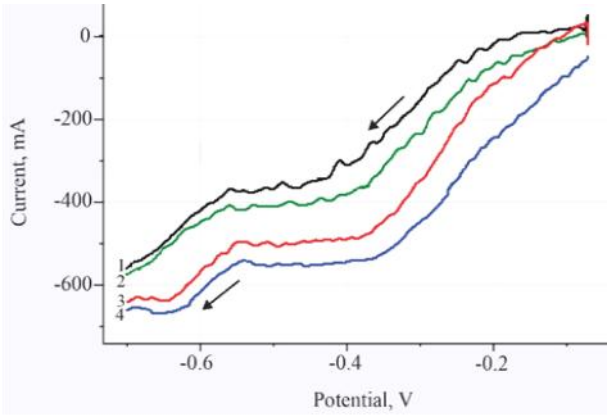

Figure 5. *Linear polarization curves of co-deposition of nickel with cobalt at different deposition temperatures. Electrolyte composition: 0.1 M $NiSO_4 \cdot 6H_2O$ + 0.1 M $NiCl_2 \cdot 6H_2O$ + 0.1 M $CoCl_2 \cdot 6H_2O$ + 0.8 M $C_2H_5NO_2$, pH adjusted to 9.5 by adding NH_4OH, ν = 15 mV s^{-1}, Temperature: 1: 298; 2: 308; 3: 313 and 4: 318 K*

Studies on the deposition of Ni-Co thin films were also conducted using a rotating disk electrode. The electrode rotation speed varied from 900 to 3600 rpm. The obtained data are presented in Figure 6a. The speed of rotation of the electrode significantly affects the rate of co-deposition of nickel with cobalt, while the wave corresponding to the reduction of cobalt disappears, and the height of the co-deposition wave increases. Apparently, this is due to an increase in the concentration of nickel ions in the near-electrode space during forced convection of the electrolyte. The dependence of the half-wave current height on the square root of the rotation speed (ω), plotted based on the data from Figure 6a, exhibits a linear character, which is characteristic of processes governed by diffusion-controlled kinetics (Figure 6b).

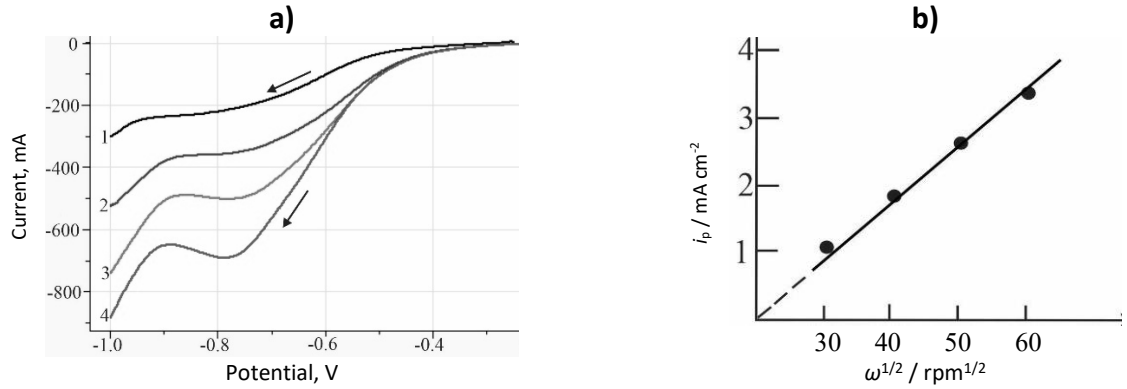

Figure 6. *a) Linear polarization curves of the co-deposition of nickel with cobalt on a rotating platinum electrode. Electrolyte composition: 0.1 M $NiSO_4 \cdot 6H_2O$ + 0.1 M $NiCl_2 \cdot 6H_2O$ + 0.1 M $CoCl_2 \cdot 6H_2O$ + 0.8 M $C_2H_5NO_2$, pH adjusted to 9.5 by adding NH_4OH, T = 298 K, ν = 0.015 V s^{-1}, 1 - 900; 2 - 1600; 3 - 2500; 4 – 3600 rpm; b) - dependence of i_p on the square root of the electrode rotation speed*

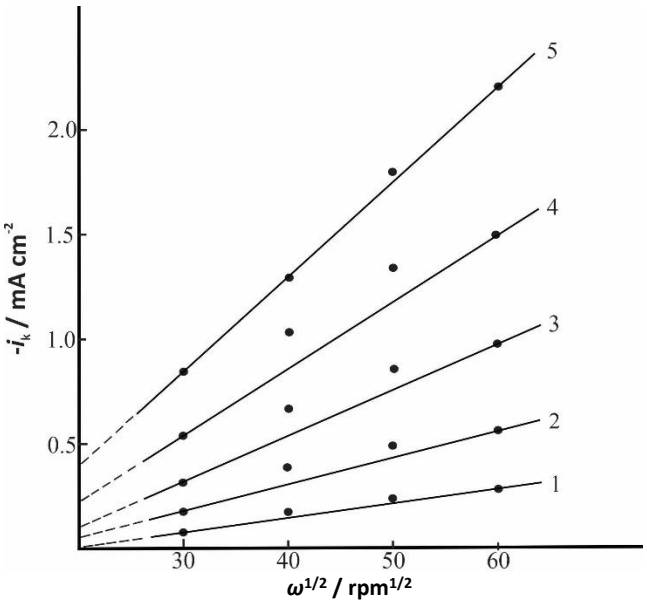

Figure 7. *Dependence of the current density on the square root of the rotation speed of the disk electrode, at potentials: 1: -0.45; 2: -0.50; 3: -0.55; 4: -0.60 and 5: -0.65 V*

When extrapolating this line, it is evident that it intersects the vertical axis at zero.

Furthermore, based on the data from Figure 6a, the dependence of the current density on the square root of the electrode rotation speed was constructed at various potentials (Figure 7). Figure 7 shows that at the onset of the co-deposition process, at a potential of -0.45 V, the limiting stage is the diffusion of depositing ions to the cathode surface (line 1 intersects the ordinate axis at zero). Subsequently, at higher potentials, the lines intersect the ordinate axis above zero, indicating that at potentials after -0.45 V, the Ni-Co co-deposition process is controlled by electrochemical polarization [37].

To study the properties of Ni-Co thin films, they were deposited on nickel substrates using the galvanostatic method. Electrolysis was carried out from an electrolyte containing 0.1 M $NiSO_4 \cdot 6H_2O$ + + 0.1 M $NiCl_2 \cdot 6H_2O$ + 0.1 M $CoCl_2 \cdot 6H_2O$ + 0.8 M $C_2H_5NO_2$, pH adjusted to 9.5 by adding NH_4OH, with a current density of i_k = 10 to 25 mA cm^{-2}, at room temperature, and an electrolysis time of 5 to 15 hours. The thickness of the films depended on the electrolysis time and ranged from 2 to 5 μm. Since the deposited films were amorphous, they were annealed in an Ar atmosphere and in air to perform X-ray phase analysis. The deposited films contained 37.25 % Ni, 51.43 % Co and 11.32 % O_2.

Figure 8 shows the X-ray diffraction pattern of an Ni-Co film obtained by galvanostatic deposition on a nickel substrate after annealing in air. The X-ray diffraction pattern reveals two compounds-cobalt oxide (CoO) and $NiCo_2O_4$, while the lines corresponding to pure nickel are attributed to the substrate material.

Since the deposited films were amorphous, they were annealed in an Ar atmosphere and air for X-ray phase analysis. The presence of oxygen compounds of nickel and cobalt in the film composition was confirmed by SEM and EDX analyses, as shown in Figures 9 and 10. The oxygen compounds appeared in the X-ray diffraction pattern as a result of the interaction of the Co phase with oxygen from the air (CoO) and the Ni-Co phase ($NiCo_2O_4$). The formation of oxygen compounds in the films contributes to an increase in their electrocatalytic activity [38]. Figure 10 shows the morphology of the Ni-Co thin film. The obtained $NiCo_2O_4$ thin films were dark gray, finely crystalline, and had a spinel structure. The analysis data confirmed the composition of the Ni-Co film obtained from the X-ray diffraction pattern of the precipitate, which included Ni (a), Co (b), and O (c), and Figure 10a shows the microstructure of the Ni-Co film.

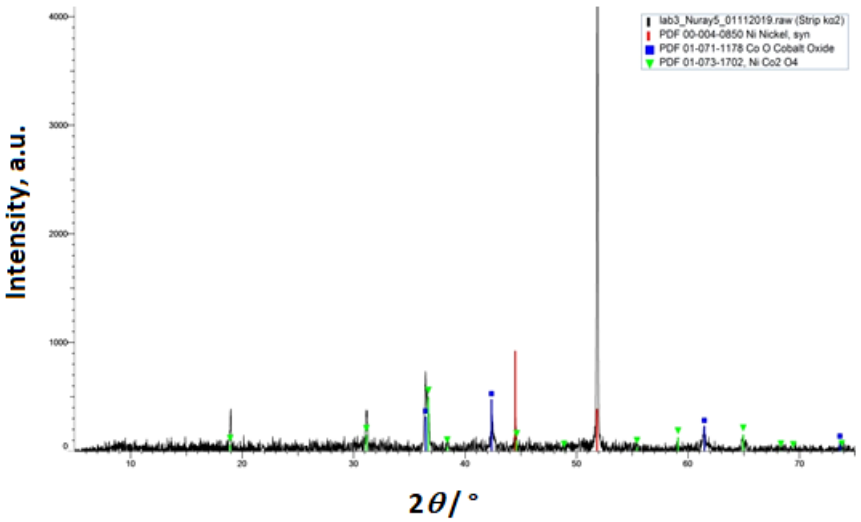

Figure 8. *X-ray diffraction pattern of the Ni-Co thin film*

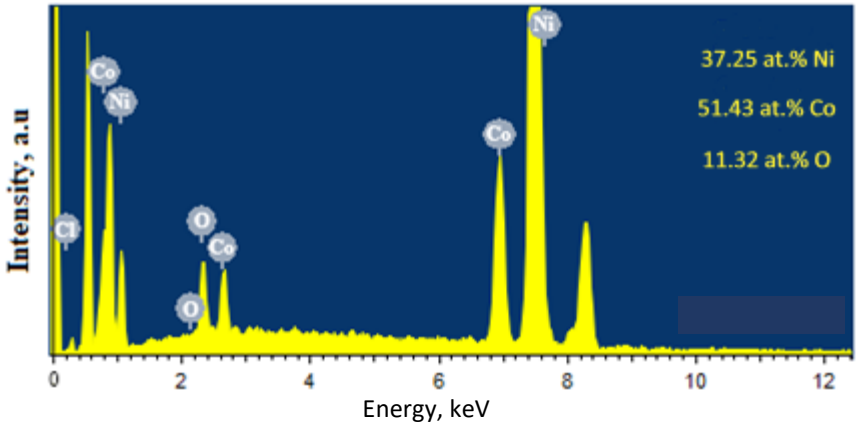

Figure 9. *Elemental composition of the Ni-Co film*

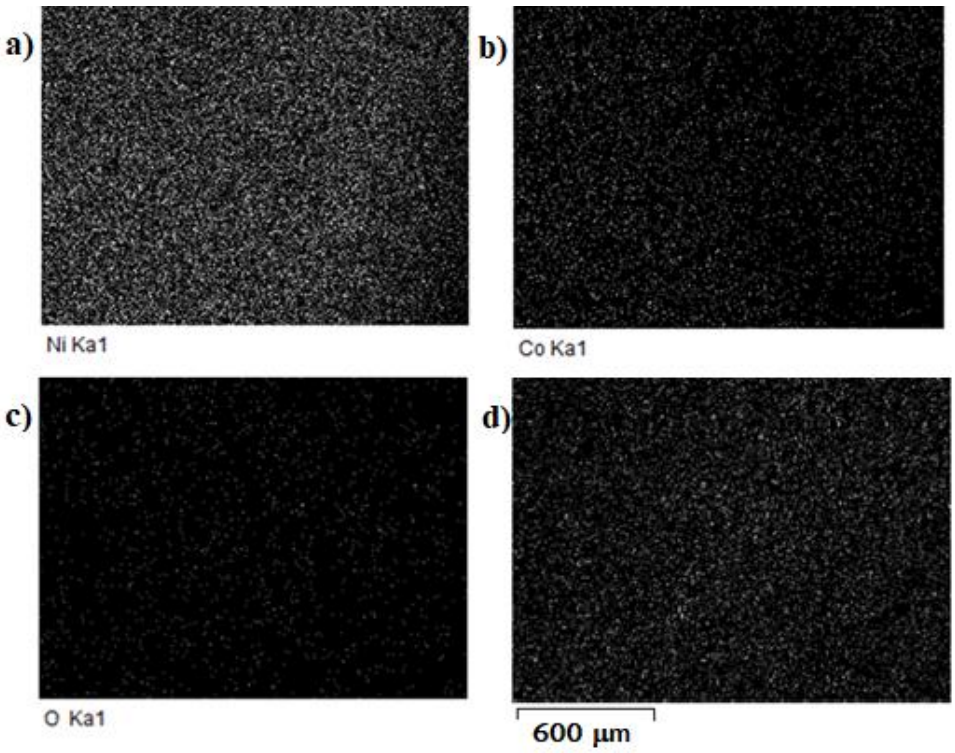

Figure 10*. SEM images of thin Ni-Co film (d) and the elements included in its composition: a: Ni, b: Co and c: O*

All three samples, both unannealed and annealed under different conditions, were investigated for electrocatalytic activity in a neutral medium during the hydrogen evolution reaction (HER). The neutral medium was chosen for the preliminary studies because it is not aggressive, and neutral electrolytes allow the use of bifunctional catalysts, simplifying electrochemical systems and significantly reducing costs. In addition, seawater can be used directly as a neutral electrolyte [39].

Figure 11 shows the electrocatalytic activity curves for the HER reaction of all three samples.

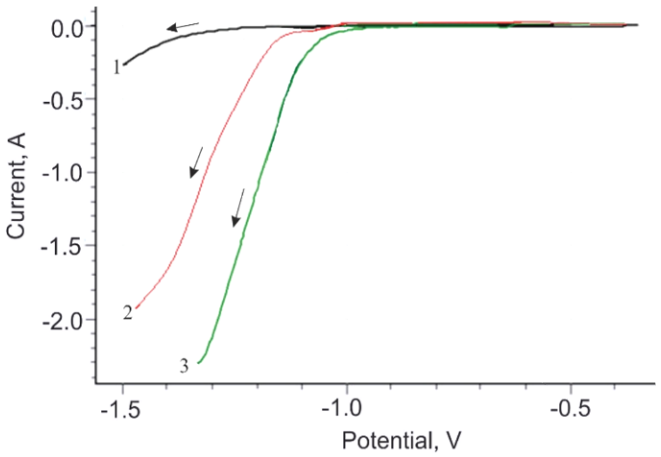

***Figure 11**. Cathodic polarization curves for HER reaction at thin Ni-Co films: 1: films annealed in an argon atmosphere; 2: films annealed in air and 3: films not annealed*

Based on the data in Figure 11, Tafel curves were constructed in the coordinates log *I vs. V,* and the catalytic activity of the electrodes was determined from their slope (tg α).

It was found that the best catalytic activity was exhibited by the unannealed amorphous samples, with a Tafel slope of 118 mV dec^{-1}, followed by the samples annealed in air, with a slope of 175 mV dec^{-1}, while the samples annealed in an argon atmosphere exhibited the lowest activity, with a Tafel slope of 210 mV dec^{-1}.

Conclusions

The study established the optimal composition of the alkaline electrolyte, into which glycine was introduced as a chelating component for the co-deposition of nickel with cobalt. It was found that the process of co-deposition of nickel with cobalt is irreversible and is controlled by the diffusion of the depositing ions in the initial stage; however, as the process progresses, it becomes controlled by electrochemical polarization. This was confirmed by recording polarization curves at various cobalt concentrations in the electrolyte and rotation speeds of the disk electrode. The process itself exhibits an anomalous nature, as, contrary to expectations, the cobalt content in the deposits exceeds that of nickel.

The thin Ni-Co films deposited under optimal conditions contained 37.25 % Ni, 51.43 % Co and 11.32 % O_2. An increase in the concentration of cobalt in the electrolyte accelerates the co-deposition process and increases its content in the deposits, while the concentration of nickel has little effect on the co-deposition process. The composition of the deposited films was found to depend on the concentration of cobalt in the electrolyte, temperature, and current density.

Electrocatalytic activity studies of the hydrogen evolution reaction showed that the best electrocatalytic properties were exhibited by the amorphous Ni-Co thin films with a Tafel slope of 118 eV dec^{-1}.

References

[1] Q.-N. Ha, N.S. Gultom, Ch.-H. Yeh, D.-H. Kuo, One-pot synthesized Li, V co-doped Ni_3S_2 nanorod arrays as a bifunctional electrocatalyst for industrialization-facile hydrogen production via alkaline exchange membrane water electrolysis, *Chemical Engineering Journal* 472 (2023) 144931. https://doi.org/10.1016/j.cej.2023.144931

[2] A. Sh. Aliyev, R. G. Guseynova, U. M. Gurbanova, D. M. Babanly, V. N. Fateev, I. V. Pushkareva, D. B. Tagiyev, Electrocatalysts for water electrolysis, *Chemical Problems* **16(3)** (2018) 283-306. https://chemprob.org/wp-content/uploads/2018/08/A.-Aliyev-283-306-1.pdf

[3] J. Feng, X. Zhong, M. Chen, P. Zhou, L. Qiao, H. Bai, D. Liu, D. Liu, Y.-Y. Chen, W. F. Ip, Sh. Chen, J. Ni, D. Liu, H. Pan, Iron-incorporated defective graphite by in-situ electrochemical oxidization for oxygen evolution reaction, *Journal of Power Sources* **561** (2023) 232700. https://doi.org/10.1016/j.jpowsour.2023.232700

[4] J. Zhou, X. Meng, P. Ouyang, R. Zhang, H. Liu, Ch. Xu, Z. Liu, Electrochemical behavior and electrodeposition of Fe-Co-Ni thin films in choline chloride/urea deep eutectic solvent, *Journal of Electroanalytical Chemistry* **919** (2022) 116516. https://doi.org/10.1016/j.jelechem.2022.116516

[5] L. Jiang, N. Yang, C. Yang, X. Zhu, Y. Jiang, X. Shen, C. Li, Q. Sun, Surface wettability engineering: CoS_x-Ni_3S_2 nanoarray electrode for improving overall water splitting, *Applied Catalysis B: Environmental* **269** (2020) 118780. https://doi.org/10.1016/j.apcatb.2020.118780

[6] B. Yang, M. Li, Z. Zhang, Sh. Chen, M. Wang, L. Sheng, L. Deng, R. Si, M. Fan, H. Chen, Spatial and electronic effects synergistically enhanced electrocatalytic oxygen evolution using atomic iridium-anchored cobalt oxyhydroxide nanosheets, *Applied Catalysis B* **340** (2024) 123227. https://doi.org/10.1016/j.apcatb.2023.123227

[7] X. Gu, Z. Liu, M. Li, J. Tian, L. Feng, Surface structure regulation and evaluation of FeNi-based nanoparticles for oxygen evolution reaction, *Applied Catalysis B: Environmental* **297** (2021) 120462. https://doi.org/10.1016/j.apcatb.2021.120462

[8] H. Zhao, Z.-Y. Yuan, Progress and perspectives for solar-driven water electrolysis to produce green hydrogen, *Advanced Energy Materials* **13(16)** (2023) 2300254. https://doi.org/10.1002/aenm.202300254

[9] T. B. Massalski, H. Okamoto, P. R. Subramanian, L. Kacprzak, *Binary Alloy Phase Diagrams-Second edition*, ASM International, Materials Park, Ohio, 1990. **ISBN:** 978-0-87170-403-0

[10] J. A. M. Oliveira, A. F. de Almeida, A. R. N. Campos, S. Prasad, J. J. I. N. Alves, R. A. C. de Santana, Effect of current density, temperature and bath pH on properties of Ni-W-Co alloys obtained by electrodeposition, *Journal of Alloys and Compounds* **853** (2021) 157104. https://doi.org/10.1016/j.jallcom.2020.157104

[11] R. Oriňáková, A. Oriňák, G. Vering, I. Talian, R. M. Smith, H. F. Arlinghaus, Influence of pH on the electrolytic deposition of Ni-Co films, *Thin Solid Films* **516(10)** (2008) 3045-3050. https://doi.org/10.1016/j.tsf.2007.12.081

[12] M. Landa-Castro, J. Aldana-González, M. G. Montes de Oca-Yemha, M. Romero-Romo, E. M. Arce-Estrada, M. Palomar-Pardavé, Ni-Co alloy electrodeposition from the cathode powder of Ni-MH spent batteries leached with a deep eutectic solvent (reline), *Journal of Alloys and Compounds* **830** (2020) 154650. https://doi.org/10.1016/j.jallcom.2020.154650

[13] Y. H. You, C. D. Gu, X. L. Wang, J. P. Tu, Electrodeposition of Ni-Co alloys from a deep eutectic solvent, *Surface and Coatings Technology* **206(17)** (2012) 3632-3638. https://doi.org/10.1016/j.surfcoat.2012.03.001

[14] Gh. B. Darband, M. Aliofkhazraei, A. Dolati, A. S. Rouhaghdam, Electrocrystallization of Ni nanocones from chloride-based bath using crystal modifier by electrochemical methods,

Journal of Alloys and Compounds **818** (2019) 152843. https://doi.org/10.1016/j.jallcom.2019.152843

[15] U. M. Gurbanova, Z. S. Safaraliyeva, N. R. Abishova, R. G. Huseynova, D. B. Tagiyev, Mathematical modeling the electrochemical deposition process of Ni-Mo thin films, *Azerbaijan Chemical Journal* **3** (2021) 6-11. doi.org/10.32737/0005-2531-2021-3-6-11

[16] U. M. Gurbanova, D. M. Babanly, R. G. Huseynova, D. B. Tagiyev, Study of electrochemical deposition of Ni-Mo thin films from alkaline electrolytes, *Journal of Electrochemical Science and Engineering* **11(1)** (2021) 39-49. https://doi.org/10.5599/jese.912

[17] Y. Chen, H. Yang, H. Feng, P. Yang, J. Zhang, B. Shu, Electrodeposition and corrosion performance of Ni-Co alloys with different cobalt contents, *Materials Today Communication* **35** (2023) 106058. https://doi.org/10.1016/j.mtcomm.2023.106058

[18] I. M. A. Omar, M. Aziz, Kh. M. Emran, Impact of ionic liquid [FPIM]Br on the electrodeposition of Ni and Co from an aqueous sulfate bath, *Journal of Materials Research and Technology* **12** (2021) 170-185. https://doi.org/10.1016/j.jmrt.2021.02.066

[19] W. Li, J. Hao, S. Mu, W. Liu, Electrochemical behavior and electrodeposition of Ni-Co alloy from choline chloride-ethylene glycol deep eutectic solvent, *Applied Surface Science* **507** (2020) 144889. https://doi.org/10.1016/j.apsusc.2019.144889

[20] B. Tury, M. Lakatos-Varsányi, S. Roy, Ni-Co alloys plated by pulse currents, *Surface and Coatings Technology* **200(24)** (2006) 6713-6717. https://doi.org/10.1016/j.surfcoat.2005.10.008

[21] J. Feng, L. Qiao, C. Liu, P. Zhou, W. Feng, H. Pan, Triggering efficient reconstructions of Co/Fe dual-metal incorporated Ni hydroxide by phosphate additives for electrochemical hydrogen and oxygen evolutions, *Journal of Colloid and Interface Science* **657** (2024) 705-715. https://doi.org/10.1016/j.jcis.2023.11.167

[22] W. Li, J. Hao, W. Liu, S. Mu, Electrodeposition of nano Ni-Co alloy with (220) preferred orientation from choline chloride-urea: Electrochemical behavior and nucleation mechanism, *Journal of Alloys and Compounds* **853** (2021) 157158. https://doi.org/10.1016/j.jallcom.2020.157158

[23] C. Lupi, D. Pilone, Electrodeposition of nickel-cobalt alloys: the effect of process parameters on energy consumption, *Minerals Engineering* **14(11)** (2001) 1403-1410. https://doi.org/10.1016/S0892-6875(01)00154-6

[24] D. V. Burlyaev, A. E. Tinaeva, K. E. Tinaeva, O. A. Kozaderov, Electrodeposition of zinc-nickel coatings from glycine-containing ammonium-chloride electrolyte, *Protection of Metals and Physical Chemistry of Surfaces* **56(3)** (2020) 552-559. https://doi.org/10.1134/S2070205120030077

[25] N. R. Abishova, U. M. Gurbanova, R. G. Huseynova, A. Sh. Aliyev, Electrodeposition of cobalt from alkaline glycine electrolyte, *Azerbaijan Chemical Journal* **2** (2022) 113-120. https://doi.org/10.32737/0005-2531-2022-2-113-120

[26] N. R. Abishova, G. S. Aliyev, U. M. Gurbanova, Y. A. Nuriyev, S. A. Huseynova, Study of electrodeposition of nickel from alkaline glycine electrolytes, *Azerbaijan Chemical Journal* **4** (2021) 20-24. https://doi.org/10.32737/0005-2531-2021-4-20-24

[27] M. Schwartz, N. V. Myung, K. Nobe, Electrodeposition of Iron Group-Rare Earth Alloys from Aqueous Media, *Journal of The Electrochemical Society* **151(7)** (2004) 468-477. https://doi.org/10.1149/1.1751196

[28] N. V. Sotskaya, O. V. Dolgikh, Nickel electroplating from glycine containing baths with different pH, *Prototection of Metals* **44(5)** (2008) 479-486. https://doi.org/10.1134/S0033173208050123

[29] M. C. Esteves, P. T. A. Sumodjo, E. J. Podlaha, Electrodeposition of CoNiMo thin films using glycine as additive: anomalous and induced codeposition, *Electrochimica Acta* **56(25)** (2011) 9082-9087. https://doi.org/10.1016/j.electacta.2011.06.079
[30] A. J. Critelli, P. T. A. Sumodjo, M. Bertotti, R. M. Torresi, Influence of glycine on Co electrodeposition: IR spectroscopy and near-surface pH investigations, *Electrochimica Acta* 260 (2018) 762-771. https://doi.org/10.1016/j.electacta.2017.12.032
[31] V. P. Graciano, I. Susana, C. de Torresi, Co-Ni anomalous codeposition studies: mechanism and effects of glycine, *ECS Meeting Abstracts* **02(20)** (2017) 994. https://doi.org/10.1149/MA2017-02/20/994
[32] A. Brenner, *Electrodeposition of Alloys. Principle and Practice*, Academic Press, New York, 1963.
[33] A. N. Correia, S. A. S. Machado, Anodic linear sweep voltammetric analysis of Ni-Co alloys electrodeposited from dilute sulfate baths, *Journal of Applied Electrochemistry* **33** (2003) 367-372. https://doi.org/10.1023/A:1024457930014
[34] N. Zech, E. J. Podlaha, D. Landolt, Anomalous Codeposition of Iron Group Metals: I. Experimental Results, *Journal of The Electrochemical Society* **146(8)** (1999) 2886-2891. https://doi.org/10.1149/1.1392024
[35] A.E. Angkawijaya, A.E. Fazary, S. Ismadji, Y.H. Ju, Cu(II), Co(II), and Ni(II)-antioxidative phenolate-glycine peptide systems: an insight into its equilibrium solution study, *Journal of Chemical & Engineering Data* **57(12)** (2012) 3443-3451. https://doi.org/10.1021/je300589r
[36] U. Lačnjevac, B.M. Jović, V.D. Jović, Electrodeposition of Ni, Sn and Ni-Sn alloy coatings from pyrophosphate-glycine bath, *Journal of The Electrochemical Society* **159(5)** (2012) 310-318. https://doi.org/10.1149/2.042205jes
[37] N.V. Krstajić, Lj. Gajić-Krstajić, U. Lačnjevac, B.M. Jović, S. Mora, V.D. Jović, Non-noble metal composite cathodes for hydrogen evolution. Part I: The Ni-MoO_x coatings electrodeposited from Watt's type bath containing MoO_3 powder particles, *International Journal of Hydrogen Energy* **36(11)** (2011) 6441-6449. https://doi.org/10.1016/j.ijhydene.2011.02.105
[38] Yu. V. Pleskov, V. Yu. Filinovskii, *The rotating disc electrode*. Consultants Bureau Plenum, New York, USA, 1976, p. 344. ISBN: 978-0306109126
[39] W. Li, N. Jiang, B. Hu, X. Liu, F. Song, G. Han, T.J. Jordan, T.B. Hanson, T.L. Liu, Y. Sun, Electrolyzer design for flexible decoupled water splitting and organic upgrading with electron reservoirs, *Chem* **4(3)** (2018) 637-649. https://doi.org/10.1016/j.chempr.2017.12.019